TECHNISCHE MECHANIK
an open access journal

journal homepage: www.ovgu.de/techmech

Tech. Mech., Vol. 40, Is. 2, (2020), 111–119

Received: 29.10.2019
Accepted: 25.01.2020
Available online: 06.04.2020

Comparison of the dynamics of a Duffing equation model and experimental results for a bistable cantilever beam in magnetoelastic energy harvesting

Max-Uwe Noll[1]*, Lukas Lentz[1], and Utz von Wagner[1]

[1] Technische Universität Berlin, Institut für Mechanik, Einsteinufer 5, 10587 Berlin, Germany

Abstract: Nonlinear energy harvesting systems, consisting of a piezo cantilever beam with two additional magnets placed near the beam's free end, have received a lot of attention in the past decade. The most common approach to model this system is to discretize the beam in space with one modal ansatz function and to assume a cubic restoring force caused by the magnetic field. The magnets are positioned so that two stable equilibrium positions exist in addition to the unstable undeflected beam tip displacement, i.e. the system is bistable. This modeling procedure results in a Duffing equation with a negative linear and a positive cubic restoring term, which is capable to represent the bistability. However, its sufficiency is often just assumed without thorough experimental validation of the mentioned presumptions.
In this paper the authors present the results of broad experimental investigations into the sufficiency of the Duffing equation as the underlying model of the mechanical subsystem (beam and magnets, but for the sake of simplicity without piezos). Therefore, a model is developed accordingly, following the approach of most publications, where a heuristic method is used to determine the cubic restoring force of the system. The theoretical predictions of the Duffing like model concerning the dynamical response to different harmonic base excitations are compared to experimental measurements done on a physical setup of the investigated system. The results are generally in good agreement, however particular limitations regarding the model are observed, as there is a shift of the occurring solutions to higher frequencies in the theoretical model compared to the experiments.

Keywords: nonlinear dynamics, energy harvesting, bistable oscillator, Duffing equation, cubic restoring force

1 Introduction

The term energy harvesting describes specific strategies to derive small amounts of available energy from external sources, which would be otherwise lost. More specifically, vibrational energy harvesting systems use ambient vibrations to generate electric energy [Priya (2007), Kim et al. (2011), Erturk and Inman (2011b)]. Commonly, the mechanical energy is transferred into electric energy by the use of piezoceramics fixed on the corresponding bending structure. The tuning of such vibrating systems, as well as other strategies to increase their efficiency, have been addressed in many publications, e.g. [Adhikari et al. (2009), Erturk et al. (2009)]. Particularly due to the nature of real-world excitation processes [Lentz et al. (2017)], which can be partly stochastic or have broadband frequencies, approaches have been made to use more than the discrete base frequency of any foremost linear system [Pellegrini et al. (2013), Harne and Wang (2013), Daqaq et al. (2014), Wei and Jing (2017)]. About a decade ago [Erturk et al. (2009)] has proposed the setup in figure 1, which has received great attention.

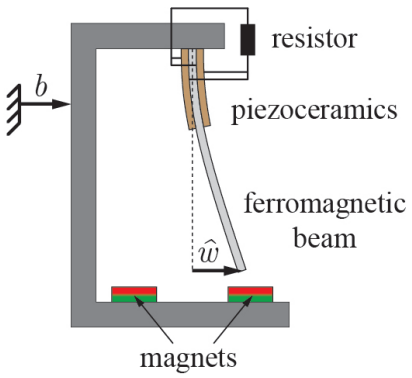

Fig. 1: Energy harvesting system. Modified figure of [Noll (2018)] with added coordinate b for the base excitation.

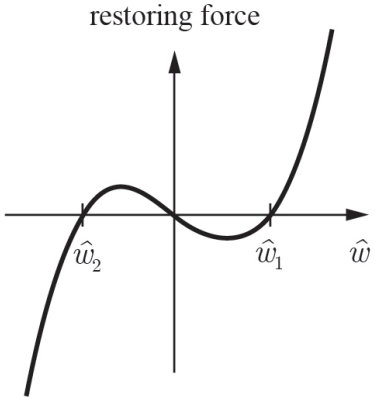

Fig. 2: Nonlinear restoring force with unstable trivial solution and two stable equilibria $\hat{w}_{1/2}$.

* E-mail address: max-uwe.noll@tu-berlin.de
doi: 10.24352/UB.OVGU-2020-019

It consists of a base frame and a ferromagnetic cantilever beam that bends under base excitation b, with attached piezoceramic patches. The beam is clamped to an external structure, which excites the system by its motion. A characteristic feature of this particular system is its nonlinear behavior due to the magnets near the free end of the beam. In figure 2 the nonlinear restoring force is shown with its three equilibrium positions, at which the restoring force vanishes. Only the two non-zero equilibrium positions $\hat{w}_{1/2}$ are stable, which is the reason for the system to be called bistable. It has shown, as many other nonlinear systems, to be superior in efficiency to its linear counterpart when the excitation is not mono frequent but somehow distributed around the system's base frequency and when the beam orbits both stable positions ([Erturk and Inman (2011a), De Paula et al. (2015)]).
In order to model this energy harvesting system, it can be divided into three subsystems which are the bending beam structure, the restoring force caused by the magnetic field induced by the permanent magnets and the electrical part, which consists of the piezoceramics and the connected electrical circuit. The basic structure of the bistable cantilever beam with magnets, but without piezoceramics, was already described in [Moon and Holmes (1979)]. This part will be referred to as the mechanical subsystem in this paper. Hence, for the sake of simplicity, no piezoceramics are considered in the modeling and in the experiment in order to have the focus on the nonlinear magnetic restoring forces.
The key component of this mechanical subsystem is the cantilever beam, which is regularly modeled as an Euler-Bernoulli beam. The beam is discretized by its first linear eigenfunction (without magnets). This modeling has become the standard approach to describe its dynamics by a single second order ordinary differential equation, which has been applied many times (as in [Litak et al. (2010), Tam and Holmes (2014), De Paula et al. (2015), Noll et al. (2019a)]). The question if more than one ansatz function is necessary, is addressed in another paper by the authors [Noll et al. (2019b)]. Its conclusions are that the use of the first linear eigenfunction of the beam is suitable in most cases and the second linear ansatz function only has a small geometric share in cases of super harmonic responses. Following the standard modeling procedure, the magnets are replaced by a single transverse force that is applied at the tip of the beam and is assumed to be of a cubic polynomial type with vanishing quadratic term. This results in the Duffing equation with negative linear and positive cubic restoring force (see e.g. [Lentz (2018)]), which is a minimal model to describe bistability. A lot of varied systems with different arrangements of magnets (see e.g. Westermann et al. (2013); Lan and Qin (2017)]) or even other nonlinear mechanisms finally end in a Duffing equation. Most of the publications about comparable bistable configurations follow this approach, or simply state a Duffing equation as the underlying model, as in [Litak et al. (2010)] or [Lentz and von Wagner (2015)]. The model parameters are then found heuristically in a manner described in the following. The displacement of the nontrivial equilibrium positions and the corresponding frequency of free vibration of small amplitude are needed. They provide the necessary information to determine the restoring parameters. This can (only) be done when an experimental setup exists, or corresponding assumptions regarding the system are made.
In [Noll et al. (2019a)] the authors have tried to apply an alternative procedure, where no existing experimental setup would be needed to determine a model by a direct computation of the restoring force. Therefore, the magnetic field was simulated by a two-dimensional FEM-approach with subsequent numeric force computation, where linear magnetic material behavior (i.e. constant permeability) is assumed. However, the resulting model in that case could not satisfyingly meet the conditions of matching equilibrium positions and corresponding frequencies. In contrast, the agreement of the equilibrium positions and frequencies are always achieved when using the aforementioned heuristic method. It yields a model that is a good approximation when the beam tip is in the vicinity of the stable equilibrium positions. However, in other ranges of the beam tip displacement, as for example the unstable equilibrium with zero displacement, this might not be a good approximation.
In this paper, dynamic experiments are described, investigating the system's steady state response for different harmonic base excitations with varying frequency and amplitude. In the following section, the experimental setup is introduced. The results will be compared to predictions of a model that is found according to the heuristic method, described in the second next section.

2 Experimental setup

The main focus is on the mechanical subsystem (figure 3) of the energy harvesting system, that consists of a cantilever beam (dimensions: $250 \times 20 \times 1$ mm) and permanent magnets (dimensions: $5 \times 20 \times 10$ mm). No piezoceramics are considered in the presented investigations, as mentioned in the introduction. The distance between the beam tip in the undeflected state and the top side of the magnets is about 6 mm and the gap between the magnets is 12.7 mm. The beam made of ferromagnetic steel is modeled according to section 3 as an Euler-Bernoulli beam and therefore mechanically characterized by its mass per length μ and bending stiffness EI. Further it is magnetically characterized by its relative permeability. There are some indications that the material of the beam is not linear regarding its magnetic properties, i.e. it shows a distinct hysteresis depending on the strength of the applied external magnetic field [Noll et al. (2019a)]. The magnets are made of NdFeB (Neodymium) with remanence $B_\mathrm{r} = 1.35$ T. The overall system has the physical properties given in table 1.

Tab. 1: Physical properties of the experimental setup (cf. figure 3).

property	**value**
first circular eigenfrequency of the beam when no magnets are present ω_0	2π 13.4 Hz
displacement of the nonzero equilibrium positions $\hat{w}_{1/2}$	+6.97 mm
(distance from the undeflected position when permanent magnets are present)	−6.97 mm
circular frequency of the oscillation in equilibrium positions with small amplitude ω	2π 14.9 Hz
	2π 14.6 Hz
damping ration with magnets in equilibrium positions D	0.0013
	0.0019

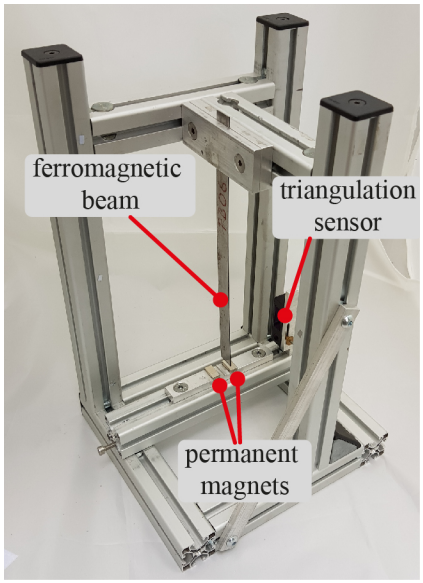

Fig. 3: Mechanical subsystem of the investigated energy harvesting system.

Note that in general there are two different circular frequencies ω for small vibrations in each stable equilibrium, due to an undesired but unavoidable asymmetry of the experimental setup. For the heuristic modeling later, the average will be taken. Same applies to the damping ratios D that are found by determining the logarithmic decrement from time signals of free beam vibrations. In order to measure the quantities in table 1, the setup shown in figure 4 is used. It consists of several devices to realize a harmonic base excitation and devices to measure the beam's response in form of its beam tip displacement. Also, the actual base excitation occurring at the base frame is measured. To determine the static (and later dynamic) displacement of the beam tip a laser triangulation sensor (ALLSENSE AM500-50) is used. It is attached to the moving base frame (cf. figure 3), hence directly provides the relative displacement of the beam tip with respect to the permanent magnets, which are fixed within the moving aluminum framework. The harmonic signal of the base excitation is generated by MATLAB R2018a and further processed by a measurement box (Datatranslation DT9837A) that provides the desired voltage signal for a shaker (LDS V406/8-PA100E) after amplification (LDS PA 100E Power Amplifier). The shaker is attached to a vibration table, containing four leaf springs as support, on which the system in figure 3 is placed. The vibration table has a notable dynamic of its own, which has an influence on the base excitation. The base frequency of the vibration table is about 6 Hz, which is not very far from the considered range of frequencies in experiments later. The range will be 7 Hz to 18 Hz and is chosen around the first eigenfrequency of the beam of 13.4 Hz. Hence, the transfer function of the vibration table is not constant within the considered range of frequencies and needs to be regarded. The measurement box provides a voltage signal that is amplified and provided to the shaker.

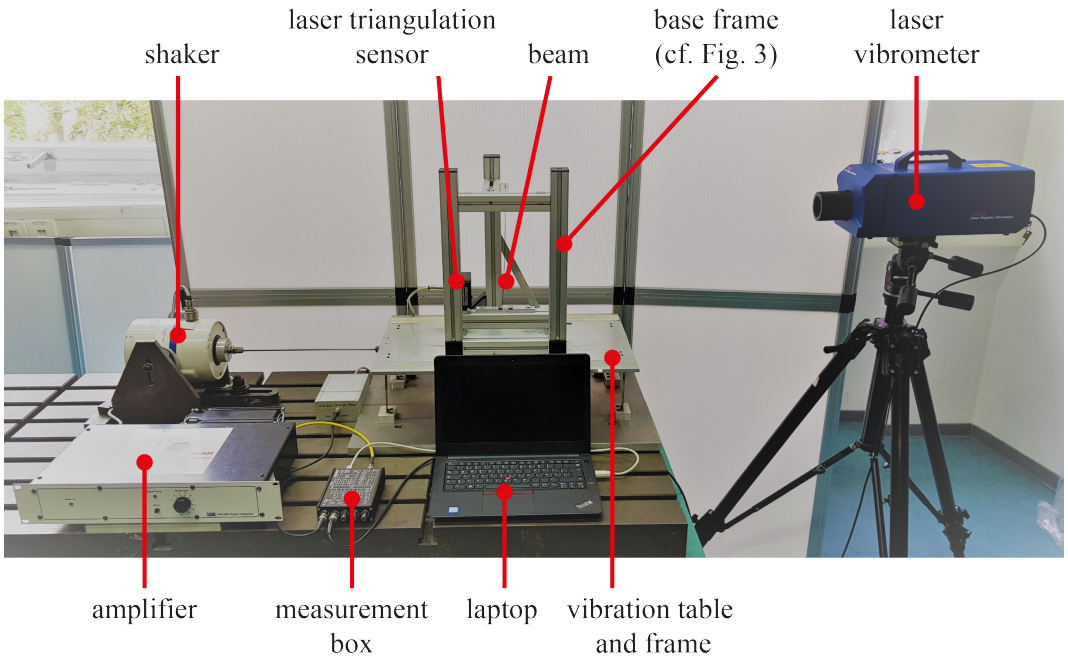

Fig. 4: Experimental setup of the energy harvesting system placed on a vibration table excited by a shaker, with measurement devices and related data acquisition tools.

The shaker generates a force proportional to this signal, to excite the vibrating table. Since a harmonic base excitation of a certain amplitude A is desired, that is independent of the circular excitation frequency Ω, the signal provided by the measurement box needs to regard the dynamics of the vibration table. To confirm that the specified signal of the excitation concurs with the actual base motion it is measured by a laser vibrometer (OptoMET Nova Basis), that determines the velocity $\dot{b}$ of the base frame. The base excitation, that is proportional to the acceleration $\ddot{b}$, is then found from this measurement by a numerical differentiation of the time signal of the discrete velocity values. The reason it is measured is that the base excitation occurring at the base frame is not always concurring with the specified signal generated in MATLAB. There is a bias in magnitude and a phase shift of roughly πrad originating from the dynamics of the vibration table. Also, the authors have observed that there are cases in which the beam, due to its inertia, has a retroactive effect on the actual base excitation. Especially when the beam tip exhibits large orbits around both of its stable equilibrium positions, deviations of the actual base excitation from the desired specified signal are probable. The measurements later to be shown in detail are chosen due to their fairly harmonic base motion.
All measurements are done in the steady state of the system, which is assumed to be reached after a 60 seconds transient response of the system. Subsequently the measurements are done for 10 seconds with a sample rate of 10 kHz. The sampling is performed after a suitable lowpass filter applied by the measurement box.

3 Modeling of the mechanical subsystem

The different aspects of the overall system can be, to a certain extent, modeled separately and in different levels of complexity. Two existing publications of the authors deal with particular parts of the energy harvesting system which are: first, the magnetic field, the thereby caused magnetic restoring force and the resulting corresponding stationary behavior of the system (equilibrium positions and corresponding frequencies of small free vibrations) in [Noll et al. (2019a)] and second, the spatial discretization of the beam using only the first linear eigenfunction of the beam in [Noll et al. (2019b)]. In both publications the beam has been modeled as an Euler-Bernoulli beam structure, that bends under excitation. The beam displacement is described by a partial differential equation for the beam displacement w depending on the beam coordinate ξ and time t as given in many continuum dynamics textbooks. Following the classical discretization process as in [Noll et al. (2019a)], the mixed Ritz ansatz

$$w(\xi, t) = x(t)\,\phi(\xi), \tag{1}$$

where x is the time dependent modal coordinate. ϕ is the first eigenfunction of the linear beam, $\xi \in [0, L]$ the beam coordinate and L the total length of the beam. ϕ is chosen to be 1 at $\xi = L$, hence x concurs with the beam tip displacement $\hat{w} = w(L, t)$ (cf. figure 1). It yields the ordinary differential equation of motion given by

$$\ddot{x}(t) + 2D\omega\dot{x}(t) - \alpha x(t) + \beta x^3(t) = g\ddot{b}(t). \tag{2}$$

Compared to [Noll et al. (2019a)] the term on the right-hand side is added, since in this paper dynamic experiments of the driven Duffing oscillator are performed considering a base excitation, while in [Noll et al. (2019a)] the static behavior and free vibrations were investigated. The coefficient g is determined accordingly and given by

$$g = -\frac{\int_0^L \phi(\xi)\,\mathrm{d}\xi}{\int_0^L \phi^2(\xi)\,\mathrm{d}\xi}. \tag{3}$$

The excitation is chosen to be a base excitation of a constant amplitude A of the form $\ddot{b}(t) = A\cos\Omega t$.
In order to get the specific kind of restoring term, that is $-\alpha x(t) + \beta x^3(t)$, the assumption has been made that the magnetic force is a cubic polynomial of the beam tip displacement. Further, a linear modal damping has been inserted with the damping ratio D. In cases where α and β are both positive, bistability is existent with the two nontrivial equilibrium positions $x_{1/2}$ on each side of the undeflected beam position

$$x_{1/2} = \pm\sqrt{\frac{\alpha}{\beta}}. \tag{4}$$

Further, if considering oscillations within these two equilibrium positions with small amplitude the circular frequency for free vibrations in each of the stable equilibrium position can be determined after linearization by

$$\omega = \sqrt{2\alpha}. \tag{5}$$

When a physical setup is available the model parameters can be determined and are given in table 2 for the setup in figure 3.

Tab. 2: Model parameters of corresponding experimental setup given table 1.

parameter	ω [1/s]	D [−]	α [1/s^2]	β [1/s^2]	g [1/m]
value	92.7	0.0016	4275.6	$8.8 \cdot 10^7$	−1.57

The parameter ω and D are found as the average of their values from an analysis of the time signals of free beam vibrations in each stable equilibrium when the magnets are applied. Even though the beams's circular eigenfrequency $\omega_0 = 2\,\pi 13.4\ 1/\mathrm{s}$ has no direct significance for the setup with magnets, it is taken to define the frequency ratio η as

$$\eta = \frac{\Omega}{\omega_0}, \tag{6}$$

which is used later. α and β are found according to (4), (5) and g by equation (3). This approach is of a heuristic nature and therefore an experimental setup needs to be present first to find the according model parameters. This is an essential drawback of this approach, since these quantities need to be measured every time the setup is changed (e.g. the distance between the magnets). On the other hand, an advantage is that the model gives a good approximation of the physical setup when the beam tip is near one of the stable equilibrium positions. The approach ensures, that the equilibrium as well as the corresponding frequency of the model concur with those of the setup (except for possible asymmetries which cannot be covered by an uneven cubic force model). In the next section the experimental results are presented, and a comparison is done to the predictions of the Duffing model.

4 Experimental results and comparison to theory

In this section experimental results are shown and compared to the predictions provided by the corresponding Duffing model equation (2) with parameters in table 2. The setup is excited by different harmonic base excitations, which differ in acceleration amplitude and frequency. The beam tip displacement is measured, as well as the actual excitation. It is common to look at the phase diagram of the solution, which is a trajectory in the state space, that shows the velocity of the beam tip over the beam tip displacement (see figure 5). For that, the beam's velocity is to be determined from the measurement of the beam tip displacement, which is achieved by a numerical differentiation done using the central difference quotient. Since the signal of the beam tip displacement is noisy and a numerical differentiation increases noise, it is necessary to lowpass filter the signals. This is done using a Butterworth lowpass filter with cut-off frequency of 90 Hz (5 times the largest excitation frequency). This frequency is chosen as a compromise between a low cut-off frequency to get smooth results and a high cut-off frequency to remain the characteristics of the phase trajectory. Also, sub and super harmonics are to be expected. The super harmonics, which can be several multiples of the excitation frequency, could be eliminated by a filter with a too low cut-off frequency.
The solution that occurs depends on the initial conditions since the system is nonlinear, what means that for one excitation different types of solutions are possible. One approach to distinguish different solutions is to consider the turning points of the beam tip throughout the measurement time. In figure 5 the turning points are marked. More specifically: when the velocity changes in sign, the beam is changing the direction it travels. If all those occurring turning points (and therefore all beam tip displacements also) have the same sign (either all exclusively positive or negative) the solution is called intrawell (in blue). If the sign switches periodically with a period not being larger than a defined threshold, the solution is labeled as interwell solution (red). If there is a very large number of turning points (in this work set to be greater than 25) with positive and negative signs the solution is considered to be chaotic, even though it might be possible it is a periodic solution with a very large period.

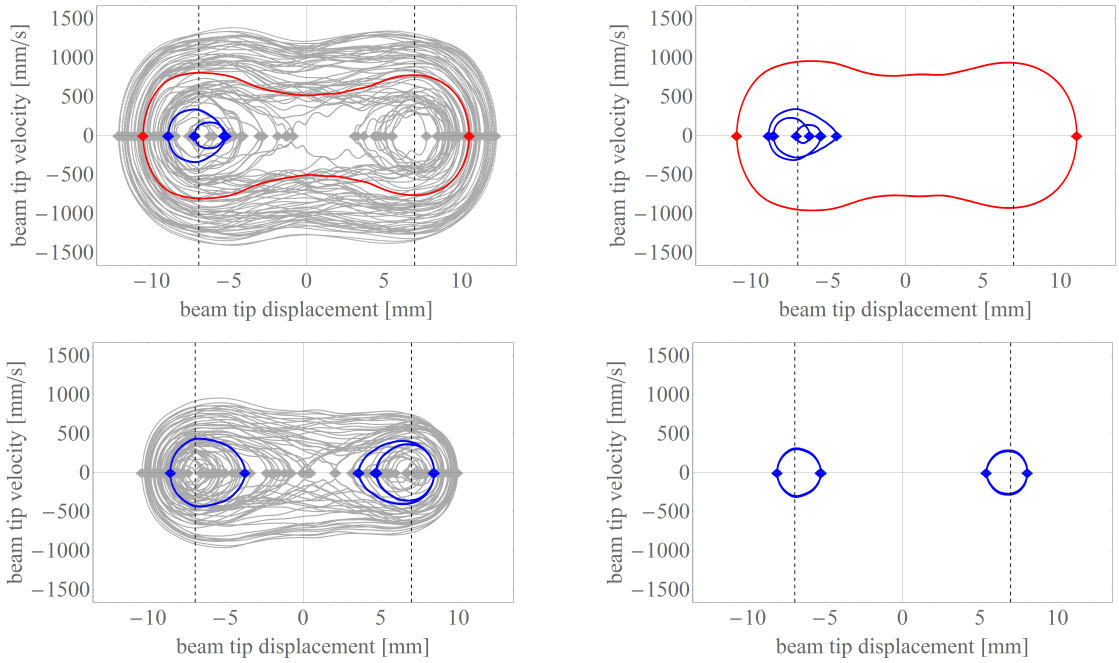

Fig. 5: Experimental phase diagrams and turning points (marker) of different solutions for a harmonic acceleration of amplitude $A = 3.81\ \mathrm{m/s^2}$ and different excitation frequencies. Upper left: 7 Hz / $\eta \approx 0.52$; upper right: 8.5 Hz / $\eta \approx 0.64$; lower left: 14 Hz / $\eta \approx 1.05$; lower right: 17 Hz / $\eta \approx 1.27$. Color code refers to the type of solution: intrawell solutions in blue, interwell solutions in red and chaotic solutions in gray.

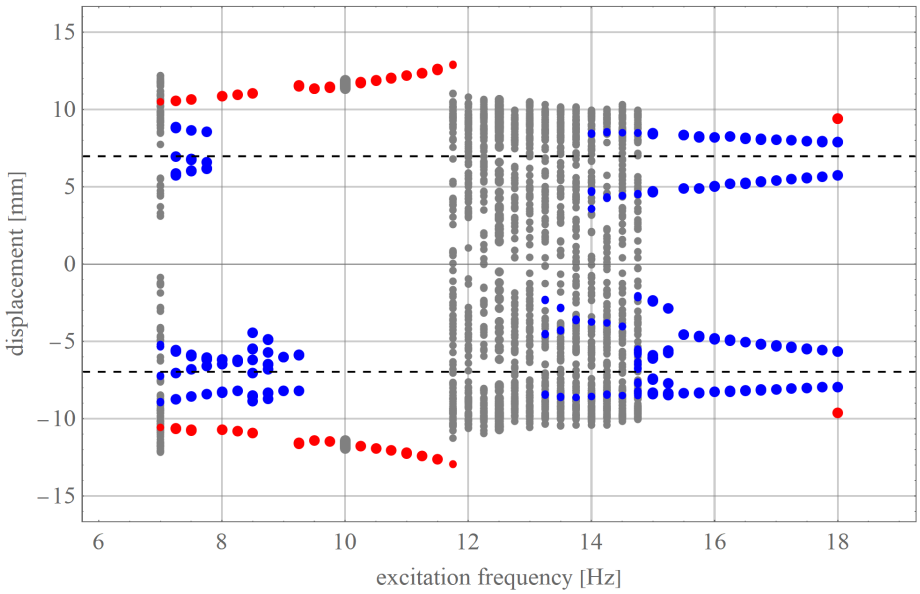

Fig. 6: Experimental results: turning points of the beam tip for parallel existing steady state solutions for harmonic acceleration of constant amplitude $A = 3.81\ \mathrm{m/s^2}$ and different excitation frequencies. Color code corresponding to figure 5.

Another possible way of displaying the occurring types of solutions is the system response diagram in figure 6, which is especially suitable to show the influence of the excitation frequency and is also used e.g. in [Lentz (2018)]. It shows all turning points of different solutions that exist in parallel for excitations of different frequency but constant amplitude. As it can be seen, there are different frequency ranges where more than one solution exists and some ranges, where only one solution has occurred during the different experimental repetitions. For each frequency ten experiments have been made, sometimes having the same final steady state and sometimes having different final steady states. The initial conditions of each experiment are not known nor reproducible, which means they cannot be controlled. Hence, it is not possible to directly reproduce each experiment numerically, making a comparison of the experiment to the Duffing model difficult. To deal with the lack of controllability of the entirety of the occurring solutions in the experiments (and also numerics), many trials with different initial conditions are done to increase the chances of various solutions, to allow a comparison between experimental and numerical results.
In figure 7, the results of numerical simulations of the model in equation (2) can be seen. It is found by a numerical integration using the NDSolve-function of MATHEMATICA 11 with no changes of the default settings with respect e.g. to the integration scheme, step size and precision goal. To get a better numerical conditioning, the differential equation for the modal coordinate x is transformed to be in the magnitude of millimeter $\tilde{x} = 10^{-3}x$ before solving for $\tilde{x}$ and transforming back. The sets of initial conditions in this case need to be chosen and are set to be 126 different equidistant values for $\tilde{x}$ for $t = 0$ between -15 and 15 and zero velocity. The integration time is 1000 seconds and the last ten seconds are used to be analyzed for their turning points analogous to the experimental data. For avoiding large arguments in the periodic cosine function and corresponding errors, the values are set back in the range between 0 and 2π when exceeding this range.

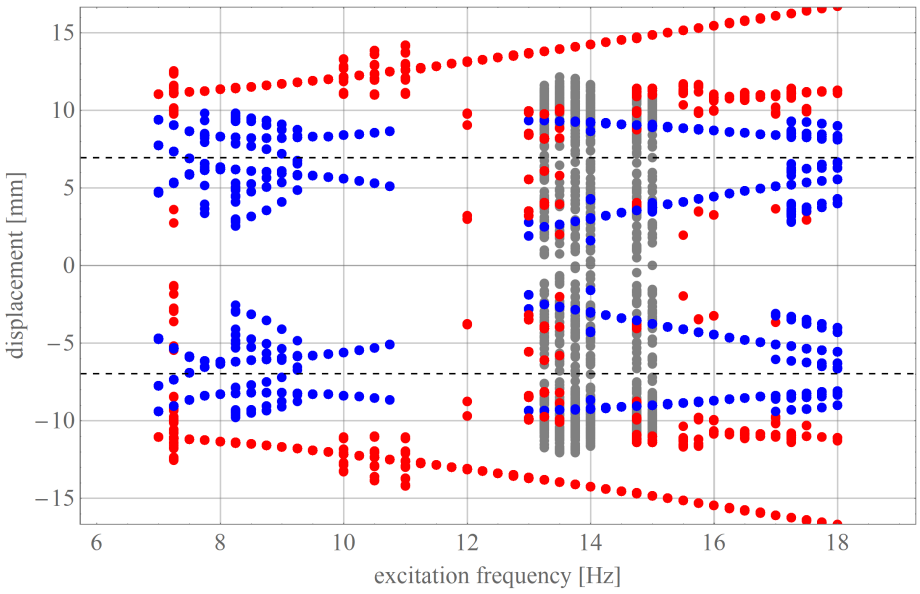

Fig. 7: Numerical results: system response diagram in Fig. 6 found by numerical integration of the Duffing model. Color code corresponding to figure 5.

When comparing both outcomes in figure 6 and 7 similar characteristics can be seen. In both diagrams, there are three main frequency ranges distinguishable: one at lower frequencies, where mostly intra- and interwell solutions (blue and red) occur in parallel, another range, where interwell solutions (only red) exist solely and a third where chaotic solutions are probable and also intrawell and interwell occur again. A difference between both diagrams is that in theory those three regions are shifted to higher frequencies. In the experiment lower excitation frequencies (around about 10 Hz / $\eta \approx 0.75$) lead to the preferred large interwell solutions and in theory, this range is slightly shifted to larger frequencies (around about 12 Hz / $\eta \approx 0.9$). The position of this range is of high interest due to its high potential for energy harvesting purposes since the beam undergoes large periodic deformations that cause high energy outputs. It is also noteworthy that the biggest region, where chaotic solutions were observed, in experiment is around the eigenfrequency of the beam (13.4 Hz / $\eta = 1$) and in theory again shifted to the right for larger frequencies (14Hz / $\eta \approx 1.05$). Another difference is that in theory large interwell solutions occur for every considered frequency but do not occur as often in the experiments. It shall be noted that the experimentally realized base excitation may differ from a harmonic excitation due to different reasons explained in section 2. A measure of the amplitude of each actual base acceleration is given by the Root Mean Square (RMS) value. The mean value of the acceleration amplitude A for all experiments (ten repetitions for each of the 45 frequencies) in figure 6 is 3.81 m/s^2 and the standard deviation of all values is 0.086 m/s^2.

The results shown so far were generated for one specific amplitude of the base excitation. In the next step, different amplitudes are considered. A map of the type of the solution (color code consistent to the figures above) that occurs for a single experiment with an excitation frequency and amplitude is shown in figure 8. Again, the experimentally realized initial conditions are uncontrollable and therefore again unknown. As it can be seen, the excitation amplitude is not uniformly distributed, due to influences of the vibrating table. The actual occurring base excitation amplitude is determined by the RMS value of the measured base excitation. The same rules to distinguish the type of solution are applied.

In figure 9 equivalent results of numerical simulations are shown. Again, time integration is performed using NDSolve in Mathematica 11 with default settings. For a 1:1 comparison of the results, the same excitation and initial conditions would need to be considered. This is impossible as described above as there are very restricted possibilities to control the initial conditions in the experimental setup. For this reason, again more simulations are done as experiments to cover a broader range of initial conditions. For simulations this is easier to perform as they are not as time consuming and can be done partly parallel.

For each excitation 25 simulations are performed, where the initial conditions are equidistant displacements $x(t = 0)$ in the range of $[-3x_1, 3x_1]$ with zero velocity. Only if always the same solution occurred, a filled squared marker of corresponding color is used. If the same solution occurs between 15 and 24 times out of 25, an diamond marker of the lighter color of the solution that occurred the most is used. Further, no marker is used, if no solution appeared more than at least 15 out of 25 times. Note that, for these criteria, chaotic solutions are less likely on the map and never occur 25 out of 25 times for a certain excitation. Consequently no squared grey marker can be found, but grey diamond markers are to be seen on the map in the same regions chaos appeared experimentally.

Again, when comparing both results, similar characteristics can be found. Overall, the model is in general suitable to predict the experimental results, but in detail deviations can be found. In good agreement, for example, are the position of chaotic solutions (grey) and that for small excitation amplitudes (below 2 m/s^2), where mostly intrawell solutions exist. Differences are again shifts of the different regions to higher frequencies in the model results, as can be seen in the large red region. Similar theoretical investigations with maps of this kind can also be found in [Panyam et al. (2014)], which concur with the results of this paper.

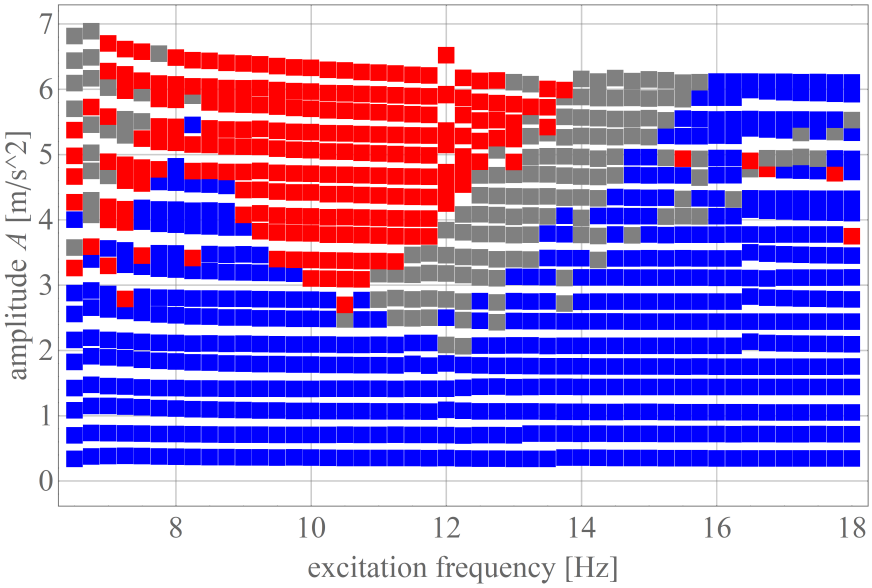

Fig. 8: Map of experimental results of the system response for different excitation frequencies and different amplitudes of harmonic acceleration. Only one experiment for each excitation is performed, wherefore only one solution occurred and uniquely defines the color of the marker. Color code corresponding to figure 5.

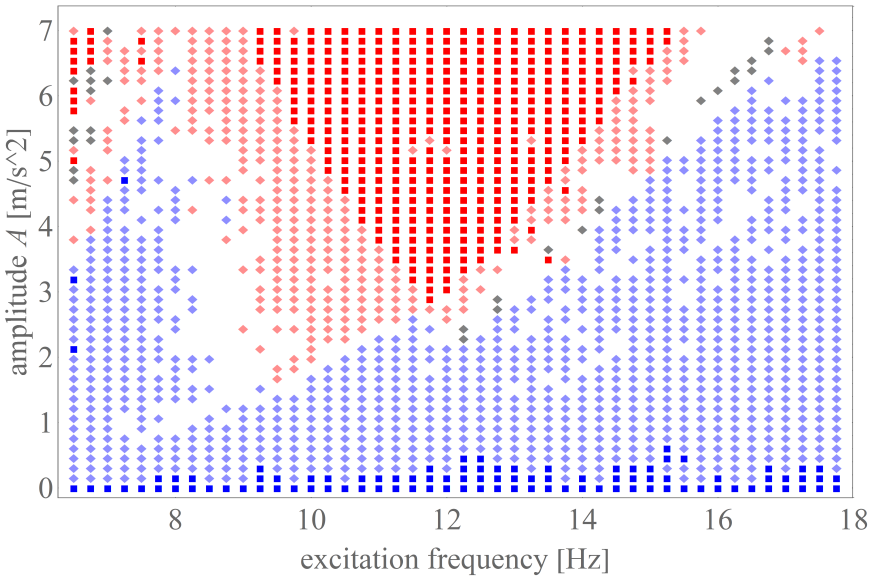

Fig. 9: Map of numerical results of the system responses found by time integration to be compared with figure 8. Color code corresponding to figure 5.

5 Conclusions

Energy harvesting performed by a bistable cantilever beam has attracted much attention in the past years. In most of the corresponding publications, the restoring force of the energy harvesting system is assumed to be of third degree, i.e. cubic. This modeling leads to the bistable Duffing equation. Corresponding model parameters are found heuristically.
In this paper, the assumption, that the restoring force is a cubic polynomial depending solely on the beam tip displacement, is investigated for suitability. Extensive experiments are performed to experimentally determine the system response for varying harmonic base excitations. A comparison to numerical results by time integration of the corresponding Duffing model is presented. The biggest issue is that the initial conditions cannot be controlled on the experimental setup that is used. Hence, the diversity of the solutions is probably not fully represented. To overcome this limitation several experiments and many simulations with varying initial conditions are done to increase the probability of occurrence of the respectively existing different solutions. In any case, the final steady solution of the system is in the focus of interest. Although there is no guarantee that all possible solutions are found, neither experimentally nor numerically, the occurring solutions are in good agreement and the results are broad enough for a comparison of the general characteristics. In fact the results show that in general the model covers most of the characteristics that can be seen in experiments but may have deviations. More specific, there might be a slight shift of the existence of solutions towards larger frequencies in theory. This might lead to false predictions when optimizing an energy harvesting system by tuning it to an existing harmonic excitation of a specific frequency. In general, the cubic restoring characteristics seems to be a good model, if the requirements on the accurateness of the model are not too high. On the other hand, as e.g. described in [Lentz (2018)] or [Noll et al. (2019a)], there may be specific cases where higher order approximations or in general extended modeling may be necessary.

6 Funding

This study was funded by Deutsche Forschungsgemeinschaft (DFG, German Research Foundation) - WA 1427/23-1,2.

References

S. Adhikari, M. I. Friswell, and D. J. Inman. Piezoelectric energy harvesting from broadband random vibrations. *Smart Materials and Structures*, 18(11), 2009. ISSN 09641726. doi: 10.1088/0964-1726/18/11/115005.

Mohammed F. Daqaq, Ravindra Masana, Alper Erturk, and D. Dane Quinn. On the Role of Nonlinearities in Vibratory Energy Harvesting: A Critical Review and Discussion. *Applied Mechanics Reviews*, 66(4):40801, 2014. ISSN 0003-6900. doi: 10.1115/1.4026278. URL http://appliedmechanicsreviews.asmedigitalcollection.asme.org/article.aspx?doi=10.1115/1.4026278.

A. S. De Paula, D. J. Inman, and M. A. Savi. Energy harvesting in a nonlinear piezomagnetoelastic beam subjected to random excitation. *Mechanical Systems and Signal Processing*, 54:405–416, 2015. ISSN 10961216. doi: 10.1016/j.ymssp.2014.08.020. URL http://dx.doi.org/10.1016/j.ymssp.2014.08.020.

A. Erturk and D. J. Inman. Broadband piezoelectric power generation on high-energy orbits of the bistable Duffing oscillator with electromechanical coupling. *Journal of Sound and Vibration*, 330(10):2339–2353, 2011a. ISSN 0022460X. doi: 10.1016/j.jsv.2010.11.018. URL http://www.sciencedirect.com/science/article/pii/S0022460X10007807.

A. Erturk and D. J. Inman. *Piezoelectric Energy Harvesting*. John Wiley & Sons, Ltd, 2011b. doi: 10.1002/9781119991151.

A. Erturk, J. Hoffmann, and D. J. Inman. A piezomagnetoelastic structure for broadband vibration energy harvesting. *Applied Physics Letters*, 94(25):254102, 2009.

R. L. Harne and K. W. Wang. A review of the recent research on vibration energy harvesting via bistable systems. *Smart Materials and Structures*, 22(2), 2013. ISSN 09641726. doi: 10.1088/0964-1726/22/2/023001.

H. S. Kim, J. H. Kim, and J. Kim. A review of piezoelectric energy harvesting based on vibration. *International Journal of Precision Engineering and Manufacturing*, 12(6):1129–1141, 2011. ISSN 12298557. doi: 10.1007/s12541-011-0151-3.

C. Lan and W. Qin. Enhancing ability of harvesting energy from random vibration by decreasing the potential barrier of bistable harvester. *Mechanical Systems and Signal Processing*, 85:71–81, 2017. ISSN 10961216. doi: 10.1016/j.ymssp.2016.07.047. URL http://dx.doi.org/10.1016/j.ymssp.2016.07.047.

L. Lentz. Zur Modellbildung und Analyse von bistabilen Energy-Harvesting Systemen. *Dissertation, TU Berlin*, 2018.

L. Lentz and U. von Wagner. Multi-mode model of a piezomagnetoelastic energy harvester under random excitation. *Pamm*, 15(1): 259–260, 2015. doi: 10.1002/pamm.201510120.

L. Lentz, H. T. Nguyen, and U. von Wagner. Energy harvesting from bistable systems under random excitation. *Machine Dynamics Research*, 41, 2017.

G. Litak, M. I. Friswell, and S. Adhikari. Magnetopiezoelastic energy harvesting driven by random excitations. *Applied Physics Letters*, 96(21):12–15, 2010. ISSN 00036951. doi: 10.1063/1.3436553.

F. C. Moon and P. J. Holmes. A magnetoelastic strange attractor. *Journal of Sound and Vibration*, 65(2):275–296, 1979.

M.-U. Noll. Energy harvesting system. *figshare*, 2018. doi: https://doi.org/10.6084/m9.figshare.7492208.v1.

M.-U. Noll, L. Lentz, and U. von Wagner. On the Improved Modeling of the Magnetoelastic Force in a Vibrational Energy Harvesting System. *Journal of Vibrational Engineering and Technologies*, (0123456789), 2019a. ISSN 25233939. doi: 10.1007/s42417-019-00159-4. URL https://doi.org/10.1007/s42417-019-00159-4.

M.-U. Noll, L. Lentz, and U. von Wagner. on the Discretization of a Bistable Cantilever Beam With Application To Energy Harvesting. *Facta Universitatis, Series: Mechanical Engineering*, 17(2):125, 2019b. ISSN 0354-2025. doi: 10.22190/fume190301031n.

M. Panyam, R. Masana, and M. F. Daqaq. On approximating the effective bandwidth of bi-stable energy harvesters. *International Journal of Non-Linear Mechanics*, 67:153–163, 2014. ISSN 00207462. doi: 10.1016/j.ijnonlinmec.2014.09.002. URL http://dx.doi.org/10.1016/j.ijnonlinmec.2014.09.002.

S. P. Pellegrini, N. Tolou, M. Schenk, and J. L. Herder. Bistable vibration energy harvesters: A review. *Journal of Intelligent Material Systems and Structures*, 24(11):1303–1312, 2013. ISSN 1045389X. doi: 10.1177/1045389X12444940.

S. Priya. Advances in energy harvesting using low profile piezoelectric transducers. *Journal of Electroceramics*, 19(1):165–182, 2007. ISSN 13853449. doi: 10.1007/s10832-007-9043-4.

J. I. Tam and P. Holmes. Revisiting a magneto-elastic strange attractor. *Journal of Sound and Vibration*, 333(6):1767–1780, 2014. ISSN 0022460X. doi: 10.1016/j.jsv.2013.11.022. URL http://dx.doi.org/10.1016/j.jsv.2013.11.022.

C. Wei and X. Jing. A comprehensive review on vibration energy harvesting: Modelling and realization. *Renewable and Sustainable Energy Reviews*, 74(November 2016):1–18, 2017. ISSN 18790690. doi: 10.1016/j.rser.2017.01.073. URL http://dx.doi.org/10.1016/j.rser.2017.01.073.

H. Westermann, M. Neubauer, and J. Wallaschek. Modeling of a nonlinear vibration-based energy harvesting system as a Duffing oscillator. *Solid State Phenomena*, 198:663–668, 2013. ISSN 10120394. doi: 10.4028/www.scientific.net/SSP.198.663.